Powder Technology 434 (2024) 119382

Contents lists available at ScienceDirect

Powder Technology

journal homepage: www.journals.elsevier.com/powder-technology

Review

Analysis of pressure fluctuations in pneumatic conveying systems via pressure sensors – A review

M. Dikty *

Schwedes + Schulze Schüttguttechnik GmbH, Apensen, Germany

HIGHLIGHTS

- Analysis methods for pulsations of horizontal conveying lines.
- Flow mode influence on pressure pulsations.
- Reasons for emergence of pressure pulsations.
- Influence of turbulence on pressure pulsations.

GRAPHICAL ABSTRACT

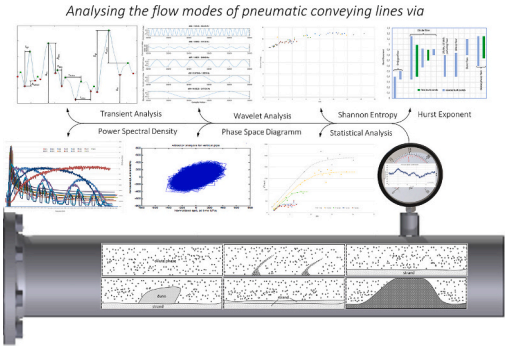

ARTICLE INFO

Keywords:
Review
Pneumatic conveying
Pulsation
Fluctuation
Turbulence

ABSTRACT

Bulk solids can usually be transported mechanically, hydraulically or pneumatically. If the choice is made for pneumatic transport, the necessary quantity of conveying gas and the necessary conveying pressure for the dimensioning of the pressure generator are decisive for the dimensioning of the system. The lower the pressure reserves selected, the more sensitively the pneumatic conveying system also reacts to pressure fluctuations. These can become so strong that the pressure generator fails due to overload. So, what are the reasons for pulsations and how can they be evaluated? Influences such as the solids loading ratio (SLR), the conveying gas velocity or the flow pattern were evaluated with a wide variety of criteria. With the aid of the pressure signal and its evaluation method, conclusions can be drawn about for example the flow condition or the degree of turbulence. This article shows the results of these research activities so far.

1. Introduction

The sand dune formation in the desert or the tornado that covers the house roof are natural occurrences of pneumatic transport. Technically, however, it is used in many applications to transport bulk solids by means of a conveying gas, usually air, through a pipeline. This takes place either in suction or pressure mode. Fig. 1 shows the schematic structure of both systems. Both systems are characterized by a negative pressure gradient in the direction of flow. The basic operations of a suction or pressure system are identical:

* Corresponding author.
E-mail address: m.dikty@schwedes-und-schulze.de.

https://doi.org/10.1016/j.powtec.2024.119382
Received 2 October 2023; Received in revised form 27 December 2023; Accepted 2 January 2024
Available online 9 January 2024

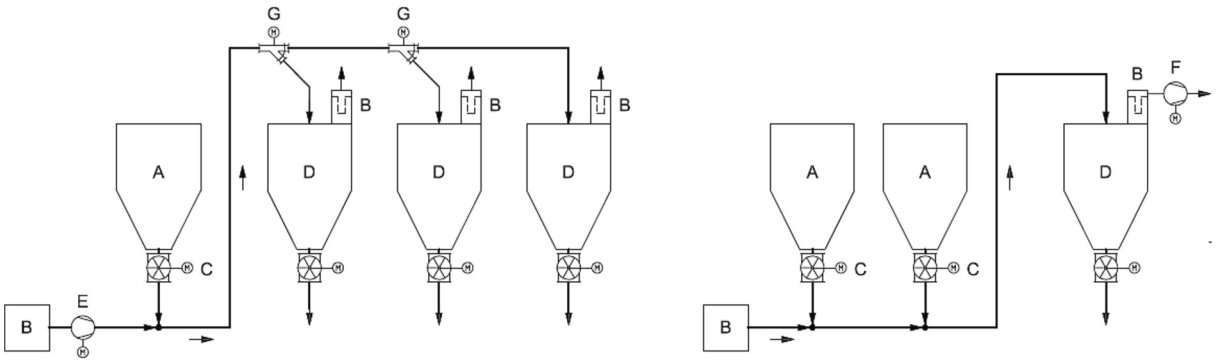

Fig. 1. Pressure system (left) / suction system (right) based on [1] with A storage silo, B filter, C feeding device, D receiving silo, E pressure generator, F vacuum generator, G conveying line diverter.

- Feeding of the bulk material into the conveying line.
- Transport through the conveying line due to a negative pressure difference from the material inlet to the outlet.
- Separation of the bulk material from the conveying gas at the receiving point (exceptions are, for example, direct reactor or burner feeding in pressure conveying, such as coal firing in the power plant or cement industry).
- Pressure generation (overpressure with pressure conveyance, negative pressure with suction conveyance).

The bulk material is fed into the conveying line in over-pressure operation by means of a rotary valve [2–6], pressure vessel [2,5,6], screw pump [2,5–8], injector (jet-feeder) [2,5,6,9], flap systems [2,5,6] or, in the case of exclusively vertical transport, by means of an airlift [2,5,6]. A suction system can operate without a feeding device. In case feeding devices are used, then rotary valves of flap systems are installed. At the receiving point, the bulk material is separated from the transport gas for further processing. This is done using cyclones and filters. In case of feeding a burner or a reactor, for example, there is no separation of the two phases.

Whether a pneumatic conveying system is used or a mechanical one is preferred depends on many criteria [10]. The decision in favour of pneumatic conveying is usually made when the conveying route is either very long or the route between the starting point and receiving point is characterized by several bends and differences in height. Further criteria in favour (+) and against (−) of pneumatic conveying are [2]:

- high adaptability of the conveying line to local conditions (+),
- environmental-friendly design (no dust emission) (+),
- feeding several receiving points with one system by conveying line diverters (+),
- low maintenance for the conveying line (+),
- use of inert gas for air-sensitive solids (+),
- conveyance of toxic and hazardous bulk materials (+),
- broad applicability for a wide variety of solids (+),
- direct transport into systems that are under overpressure (+),
- low CAPEX (capital expenditure) (+),
- less space required (+),
- carrying out chemical or physical processes during conveying (+),
- comparatively high-power requirement (−),
- wear of pipelines and feeding devices (−),
- can be used economically up to a grain size of approx. 10 mm (−),
- product degradation (−),
- dust explosion hazard (−),
- high OPEX (operational expenditure) (−),
- noise emissions from the pressure generators and, in the case of coarse and hard particles from the pipeline (−).

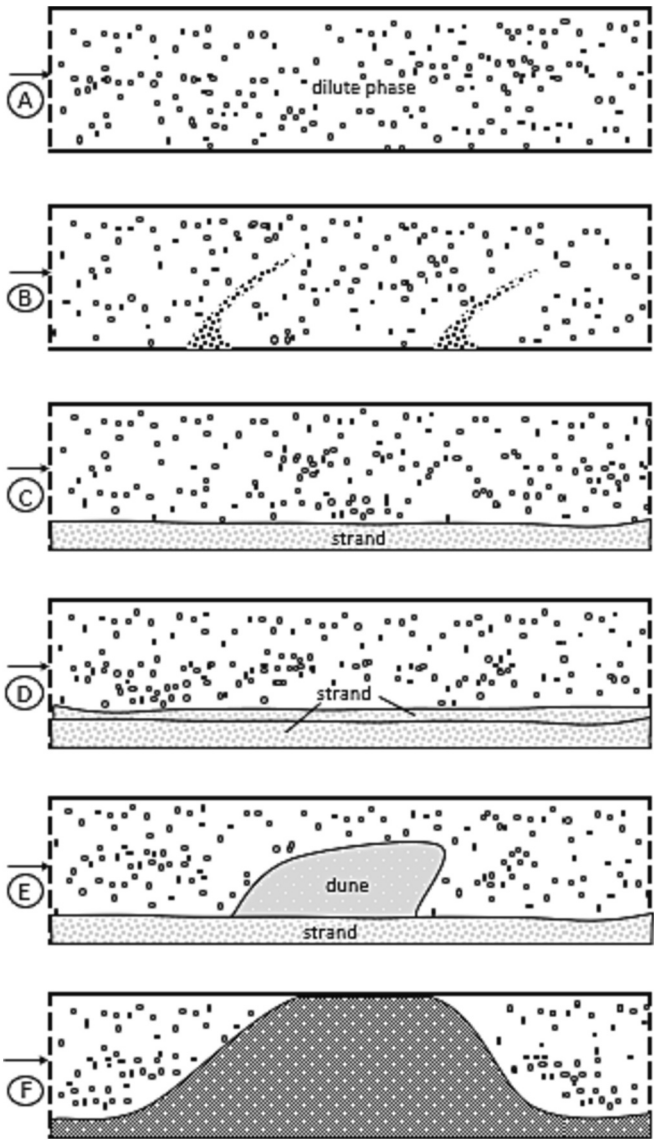

Fig. 2. Definition of flow modes in relation to [5,81].

2. Flow modes

Pressure fluctuations are often linked to the flow mode as referred to [11–17], which exists in the pneumatic conveying line and characterizes how the bulk material flows through the conveying pipe. The flow mode

is not always constant in the whole system. While for example the bulk material still flows through the pipe in the form of dunes (see definition below) at the beginning of the conveying line, for example, it can leave the conveying pipe at the end of the conveying line as a dilute flow (see definition below), depending on the system configuration. The in this review used definition of the flow modes in horizontal conveying are chosen in relation to Weber [81] and Klinzing et al. [5] and graphically depicted in Fig. 2:

Mode A – *Dilute flow*:	No strand or deposit exists. This mode is also called suspension flow, lean phase flow or homogeneous flow.
Mode B – *Blowing dunes/clusters*:	On the pipe bottom slides clusters / small dunes form out. Between the clusters particles of higher velocity flow.
Mode C – *Strand flow*:	A strand (nearly even surface), moving or not exists on the ground of the pipe.
Mode D: - *Stratified flow*:	A strand is flowing over a lower strand. The lower strand can move or not.
Mode E - *Dune flow*:	A dune (uneven surface, geometry in leaning to a sand dune) is flowing through the pipe. A lower strand (flowing or not) can exist but must not exist.
Mode F – *Plug flow*:	Plugs are flowing with low velocity through the pipe. The geometry is like a sand dune which fills the complete vertical pipe cross section. The plugs pick up bulk material at the front and lose bulk material at the end.

The naming and definition of the flow mode varies from author to author. Further flow mode overviews are shown e.g., in [2,35,48,49,82–85]. Depending on bulk material, there are other modes that can occur between mode A and F. Which flow mode occurs depends on the solid loading ratio (SLR), the velocity and the physical bulk solids data, like grain size distribution, particle density or sphericity.

In suspension flow (dilute flow), high flow velocities prevail, fine bulk materials ($d_{s,50} < 100$ µm) [6,16,68,86–89] behave here like coarse bulk materials / granules. They flow almost evenly distributed over the pipe cross-section. Irrespective of the air turbulence, the coarse particles perform a transverse movement in addition to the longitudinal movement, which is caused by the particles impacting each other and the wall. The transverse movement is essentially determined by the hardness and shape of the particles. In the case of fine-grained particles, on the other hand, the transverse movement occurs also due to the turbulence of the flow [12]. With fine-grained particles, turbulence damping of the carrier gas is observed, with coarse-grained ones an increase [14]. The particles are slowed down by the impact on walls as they bounce back and must be accelerated again. This creates a pressure loss. In the case of wall impacts, fine particles are also decelerated aerodynamically in the boundary layer. This is associated with the tendency to form deposits on the wall [15]. Particularly, clusters (Mode B) also flow through the pipeline as the flow approaches the saltation velocity.

When the transport gas velocity is reduced to/under the saltation velocity, the two-phase flow begins to separate, which is known as strand flow. Part of the solid slides as a strand on the pipe bottom, while the other part is transported flying over the strand. The strand is essentially driven by impacting particles. Compared to coarse-grained material ($d_{s,50} > 100$ µm), fine-grained material tends to form strands even at higher air velocities [12]. If the air velocity is further reduced, individual strands can push together to form dunes or plugs. Dune's flow through the conveying line like waves, as shearing forces act on the strand surface flowing on the ground.

When there is a small SLR, the transition from dune to plug conveying takes place as conveying happens over a dune situated on the ground. Dune conveyance is in the case of coarse particles and plug conveyance in the case of fine-grained bulk materials an instationary flow mode, where the risk of pipe blockages exists. Closed plugs can form which, if they are longer, eventually clog the conveying line due to the wedge action and low gas permeability of the bulk material [16]. When conveying with these conveying conditions, safe pneumatic

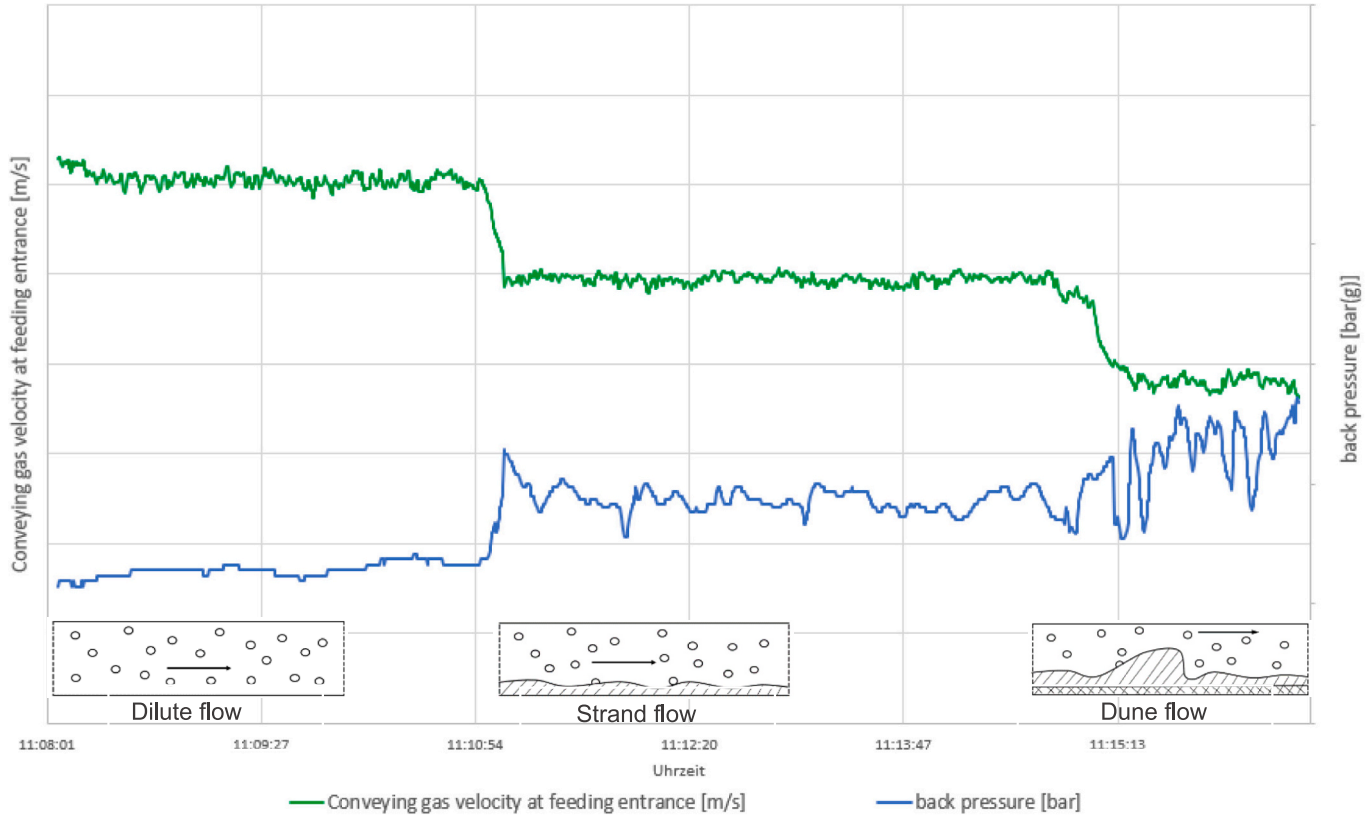

Fig. 3. Conveying trial for limestone [21], counter pressure 1.0 bar (abs.), flow mode was inspected via glass pipe 2 m after the feeding point, feeding via rotary feeder into a DN100 pipe. Total conveying distance = 152 m including 5 m vertical and seven bends.

conveying can often only be achieved with additional auxiliary equipment, such as an internal aeration pipe to increase the turbulence in the system [17]. In the case of coarse-grained goods, such wedge actions in the plug are small, so problem-free conveying can also be achieved with granules with plug conveying [12].

The flow modes and flow characteristics of fine and coarse bulk solids listed above lead to more or less strong pressure fluctuations, which are called pulsations in the following. The previous research results for pulsations in horizontal conveying pipes are considered in the following.

3. Reasons for the emergence of pulsations

Pressure fluctuations can be measured in a pneumatic conveying line with the fluid only and with bulk material. A pressure fluctuation is called a pulsation and is a rapid (short-term) pressure change in a pneumatic conveying line at a certain location. The pressure can be measured during the transition from dilute phase to strand/dune conveyance, i.e., when the saltation velocity [18–20] is undershot, bulk material sediments out of the gas stream. This bulk material is either deposited on the pipe bottom or flows unsteadily over the pipe bottom in the form of strands forming dunes at their upper surface. The flow modes and flow characteristics of fine and coarse bulk solids listed above lead to more or less strong pressure pulsations. Regarding pneumatic conveying systems, pulsations have been examined many times, primarily in order to characterize the transition from dilute phase to strand/dense phase conveying, but there is no clear definition of the term.

The pressure fluctuations/pulsations (measured as absolute or gauge pressure) in horizontal pipe sections are caused by the following effects, which are mainly listed by [35,49], which can occur independently of one another:

1. Fluctuating solids flow rate

- due to unsteady flow from the feeder (screw feeders, rotary airlocks, gate valves, venturis)

2. instationary accumulation and acceleration of solids at the feed point depending on the distance to the saltation velocity
3. air supply

- due to the nature of the air supply (e.g., pulsations due to rotating lobes in roots blower)
- pulsations due to by-pass valves and relief valves in the air supply system

4. Material transport

- interaction of particle motion with the turbulence structure

5. Line configuration

- presence of bends, diverters
- pipe material (roughness)
- total pipe length (overall pressure of the system)
- inclined pipes and combination of horizontal and vertical pipes
- pipe installations like flaps or valves
- staggered pipes

6. Collector characteristics
7. System abnormalities

- such as leakage or broken components
- electrostatic effects
- external vibrations

Fig. 3 shows an example of a pressure curve for pneumatic conveying [21]. The pressure fluctuations are explained using limestone powder ($d_{s,50} = 27$ µm, $\varrho_s = 1330$ kg/m^3). The Figure shows the initial conveying gas velocity on the left ordinate. The right ordinate shows the conveying line back pressure [bar(g)]. Both values are plotted over time. During the trial, the average mass flow was kept constant at 1.6 t/h.

The conveying tests were started with a high air velocity and thus a low SLR. Pulsations in the pressure signal at the beginning of the conveying line are very low, the flow mode can be classified as “dilute flow”.

By reducing the speed of the pressure generator, the air volume and thus the conveying gas velocity can be reduced. The SLR increases as a result. Visually it could be inspected that due to the reduction in the conveying velocity, individual particles fall out of the conveying air flow (saltation velocity is reached) and collect as strands at the bottom of the conveying pipe, and the two-phase flow separates. The strand continues to flow at reduced velocity on the pipe bottom, driven by the pressure difference across the tube element and by the momentum transfer of the impacting particles of the overflowing dilute phase flow.

It can also be seen that the pressure signal is becoming “more restless”, i.e., that the pressure fluctuations / pulsations are increasing. This is caused by the unevenly slipping and unevenly developing strands. A further reduction in the conveying velocity leads to the area of non-stationary conveying. Dunes form in places, according to the formation principles listed above. A look at the pressure curve in this time window shows that the amplitudes of the pressure fluctuations have increased but can be controlled for pneumatic conveying with sufficient pressure reserves at the pressure generator.

Fig. 3 clearly shows the results of the measurements and visual inspections of the glass pipe section at the beginning of the conveying line how the pressure fluctuations increase when the conveying gas velocity is reduced and/or the solid to air ratio increases during the transition from dilute phase mode to strand conveyance to dune conveyance.

4. Evaluation methods for assessing pulsations except pressure measurements

The following sections show the results of the efforts which were made in the field of pulsations, mainly to analyse the transition of flow modes, but also to analyse the nature of the pulsation for fine and grained bulk solids. This review gives a detailed overview of the researched results, which were obtained by using pressure sensors. Besides pressure sensors other methods were applied successfully which are reviewed here.

In the 1970th the electrical tomography was developed for the medical diagnostic [64]. Since the end of the last century, it was used to analyse two-phase flows. Dyakowski et al. [64] presents a review of the electrical tomography in 2000 where they show that ECT (electrical capacitance tomography) systems are suitable for monitoring of dry or nonconducting systems, whereas ERT (electrical resistance tomography) systems work best for wet or conducting systems. The advantage of the ERT is, that it is applicable also to dense phase systems. The results obtained in applying these tomographic devices to dense phase flow indicate the complete and dynamic patterns that are present in these systems [77].

In these century further investigations were made. Jaworski and Dyakowski [63, 64] investigated flow instabilities referred to slugs and plugs of granular materials in horizontal and vertical channels using ECT and particle image velocimetry (PIV). Williams et al. [65] investigated the transient behaviour of the internal flow structure of material pulses of fly ash.

In the Shanghai Engineering Research Centre of coal gasification several investigations were carried out, by analysing the pneumatic transport of coal, mainly under high pressure. The results of Xu et al. [66], who analysed the fluctuations of the electrostatic signal of the ECT in a dense-phase system, shows, that the dominant peak of the power

Table 1
Summary of all test facility data and bulk solids tested for the research of pulsations in pneumatic conveying systems Test rigs marked with * have vertical downstream pipe sections included.

Current no. of test centre	Reference	Pipe diameter [mm]	Pipe lenght [m]	Vertical section [m]	Bulk solid	$d_{S,50}$ [µm]	Particle density [kg/m^3]	Bulk density [kg/m^3]	Geldart-group of tested material	SLR [–]	Feeding device
	[22,24,50,53]	53	173	12.3*	Fly ash	15	2096	724	C	12–50	PV(T)
	[24,25]	50	130	12.3*	Cement	11	3000	930	C	51–70	PV(T)
1		50	130	12.3*	Fly ash	15	2096	724	C	34–85	PV(T)
	[36]	50	130	12.3*	Alumina	78	3300	1050	B	25–71	PV(T)
	[23]	53	20	–	Fly ash	19	2500	–	C	19–48	RF
		25.4	30	0	Glass bread	450	2340	–	B	2–28	SF
		25.4	30	0	Glass bread	55	2380	–	A	–	SF
		25.4	30	0	Alumina	400	3420	–	B	–	SF
2	[35]	25.4	30	0	PVC	137	1180	–	A	–	SF
		50.8	25	4.8	PS	3900	1045	735	D	2–29	RF
		50.8	25	4.8	PE	3300	1400	892	D	2–29	RF
3	[37,40]	50.8	25	4.8	Polyolefin	4600	870–940	–	D	2–29	RF
	[38]	20	34	10.8	Coal dust	36	1382	540	A	230–580	PV(B)
		20	34	10.8	Coal dust	35	1532	507	A	60–540	PV(B)
4	[39]	50	10	4	Coal dust	35	1532	507	A	99–557	PV(B)
5	[41]	36.8	26	8.3	Coal dust	61	1322	537	A	19–98	RF
6	[28–30,61,78]	76	8	0	PE	3500	1210	–	D	2–9	PV(B)
	[62]	76	8	0	Polystyrene	2900	1400	–	D	0.5–10	
7	[48]	40	14	0	plastic	190	1000	–	A/B	3–10	EF
		40	14	0	plastic	2800	1000	–	D	1–9	EF
		50	30	2.1	Polyester	3000	1400	–	D	1–6	RF
8	[49,56]	50	30	2.1	Glass bread	450	2480	–	B	1–4	RF
		50	30	2.1	Alumina	450	3750	–	B	1–4	RF
		69	168	7.0	Fly ash	30	2300	700	A	27–106	TPV(B)
9	[34,43,46]	69	148	7.0	White powder	55	1600	620	A	12–56	TPV(B)
		51	70	3.0	Fly ash	45	1950	950	A	16–52	PV(B)
		51	70	3.0	Cement	15	3060	1070	C	40–121	PV(B)
10	[45]	63	24	3.0	Fly ash	45	1950	950	A	23–41	PV(B)
		63	24	3.0	Cement	15	3060	1070	C	11–44	PV(B)
		56.3	52	–	Polystyrene	3100	1050	640	D	–	RF
11	[51]	56.3	52	–	Polyamide	2500	1140	646	D	–	RF
		56.3	52	–	Polystyrene	860	1100	630	A	–	RF
12	[79]	10	45	–	Coal	36	1350	–	A	200–550	PV(B)

SF: screw feeder, RF: rotary feeder, PV(T): pressure vessel top discharge, PV(B): pressure vessel bottom discharge, TPV(B): twin pressure vessel system with bottom discharge, EF: electromagnetic feeder.

spectrum moves towards higher frequency with the increasing gas superficial velocity. Pu et al. [67] investigated the motion process of slug flow and demonstrated that the slug moves in wave motions through the pipe with ECT and PIV. Fu et al. [69] analysed the dynamic behaviour of the particles through electrostatic sensor array. They found out, that, as the superficial gas velocity increases, the peak frequency value of the electrostatic signal increases linearly in dense-phase region, while that in dilute-phase region is nonlinear. Cong et al. [38] combined the pressure signal data and the ECT to identify the flow pattern in a horizontal pipe. With an enlarged team Cong [39] analysed the flow stabilities and instabilities over a big range of flow modes using ECT and the pressure signal.

Decomposition of fly ash density levels within the pipe cross-sectional were obtained and statistically analysed by Chen et al. [68]. Later they analysed pulses within a flow by the pulse-growth and decay segments, which represent the superficial fluidisation and deaeration processes during conveying [23]. Azzopardi et al. used the ECT to indicate that for the transport of fine coal there were two types of systematic fluctuations in the time series of mass flow rate and concentration. Azzopardi et al. [41] analysed the fluctuations in dense phase pneumatic conveying also of pulverized coal.

As mentioned above, in addition to ECT / ERT, PIV was also used to evaluate pressure or particle pulsations / fluctuations. Rinoshika and his teams used PIV technology in a variety of studies [57–61,70–74]. They measured the particle velocity and concentrations in the acceleration and fully developed regimes, with and without dune modes. Particle fluctuation velocity of a horizontal self-excited pneumatic conveying near the minimum pressure drop or multi-scale particle dynamics of low air velocity pipe flow were scope of their research. They combined their analysis for example with wavelet technology, pressure drop measurements or proper orthogonal decomposition (POD). Li et al. [73] used the PIV to investigate the particle fluctuating intensity during flowing through bends with coarse polyethylene. Unfortunately, PIV is limited due to its optical measuring method to low SLR.

The Laser Doppler Anemometer (LDA) or Phase Doppler Anemometer (PDA) is a non-intrusive method to analyse multi-phase flows. Tsuji and Morikawa [75] used it to analyse the air and solid velocity in a two-phase flow. They found out, that the particle size has great effect on the air-flow turbulence. Henthorn et al. [76] investigated the effect on the pressure drop by the particle characteristics, SLR and Reynolds number. They also investigated the velocity fluctuations in the single-phase and multi-phase flow of fine particles.

Hilgraf and Bartusch [44] investigated the mass flow pulsations of a Geldart group A coal by the evaluation of the load cell signal of the receiving bin at the end of the conveying line.

Further measuring methods like Positron emission particle tracking (PEPT), particle tracking velocimeter (PTV), inertial measurement unit (IMU), or optical fibre probe (OFP), were less used to investigate pulsations in horizontal pneumatic conveying systems.

It can be summarized that pulsation / fluctuation measurements are not only applied to the pressure but also to the air and bulk particles. There are a variety of measurement methods that have been used in addition to the pressure measurements considered here. The following review however concentrates on research related to pressure measurements in horizontal pneumatic conveying systems.

For the pressure measurement calibrated sensors are used. Sensors

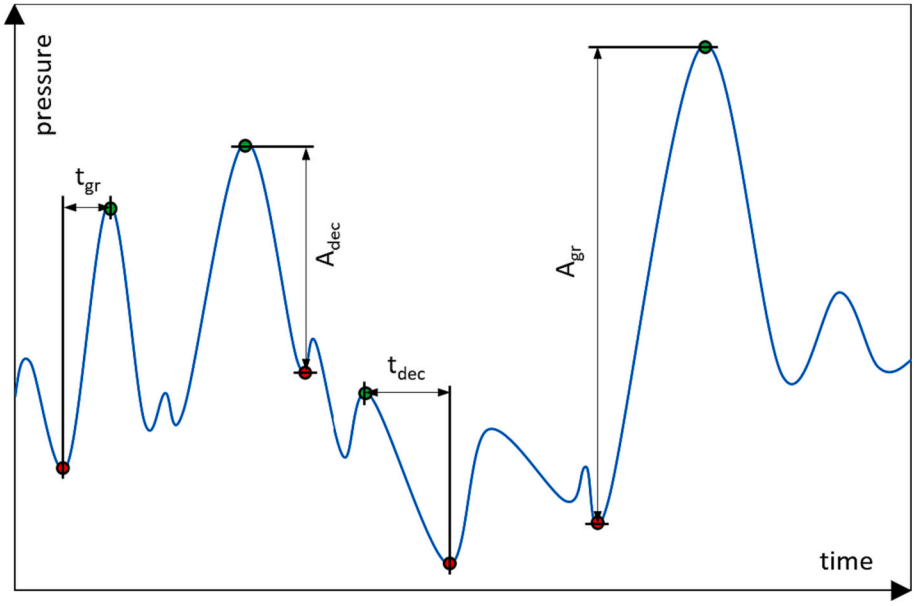

Fig. 4. Transient chart related to a static pressure signal based on [22].

can be calibrated and certified by the supplier [34,40,45,46], or the calibration must be taken place in the test rig. A procedure for the calibration is shown by Pan [92] or by Mallick [93]. Behera et al. calibrated the pressure sensor using a Barnett dead weight tester. [36].

Sensor with wear resistant flush-mounted membrane, like the PMC131 from Endress and Hauser are used by [34,45,46], they do not need a purge air connection. If sensors with for example metal membrane are used, the sensors are located reset in the socket, to avoid wear, which would influence the measured value of the pressure. Such sensors must be cleaned regularly, or purge air system were used to keep the measuring socket clean. [35,36,91] The measuring accuracies of such sensors are <0.1% of the full-scale value. [34,36,45,46] The sensors should have a sampling rate that meets the conditions of the Nyquist theorem [37,40].

5. Research results of pulsation obtained via pressure measurements in horizontal pneumatic conveying lines

As can be seen above, the term pulsation has a wide range of applications. Besides e.g., air particle pulsations or bulk material particle pulsations, the gas pressure in a pneumatic conveying line can also pulsate. The investigations carried out in this field are presented in more detail below and compared where possible. By way of introduction, Table 1 shows the test rig configuration used by the respective authors. It shows the piping data, the bulk materials used, incl. their bulk material data (bulk density, average particle diameter, particle density, and Geldart classification). In addition, the Table shows in which solid loading ratios and with which feeding device the tests were carried out. In the following, the analysis methods used so far in the analysis of horizontal pressure pulsations are presented.

5.1. Transient parameter analysis

At first the research results of the direct use of the pressure signal will be shown by transients. A transient process (lat. Transire "to go by") describes a non-stationary process. Fig. 4 shows transients applied to a static pressure signal waveform that was transient/pulsating. The pressure changes over time. However, the pressure-changes differ from each other.

The following transients are determined from Fig. 4:

- Pulse duration t_{gr}: It is the time interval between a pressure minimum and the subsequent pressure maximum [22].
- Pulse duration t_{dec}: It is the time interval between a pressure maximum and the subsequent pressure minimum [22].
- Pulse amplitude A_{gr}: It is the pressure difference between a pressure minimum and the following maximum [22,24,25].
- Pulse amplitude A_{dec}: It is the pressure difference between a pressure maximum and the following minimum [22].

The following ratios were formed from the transients including the fluid density ρ_F and the superficial gas velocity v_F [22,24,25]:

$$Slope\ of\ pulse\ growth: s_{gr} = \frac{A_{gr}}{t_{gr}} \tag{1}$$

$$Slope\ of\ pulse\ decay: s_{dec} = \frac{A_{dec}}{t_{dec}} \tag{2}$$

$$Pulse\ slope\ ratio: s_r = \frac{s_{gr}}{s_{dec}} \tag{3}$$

$$Pulse\ frequency: f_p = \frac{1}{t_{gr} + t_{dec}} \tag{4}$$

$$Non-dimensional\ pulse\ amplitude: s_{Im} = \frac{A_{gr}}{\rho_F \bullet v_F^2} \tag{5}$$

From the pulse frequency (Eq. (4)), an additional dimensionless pulse frequency was derived, comparable with the Strouhal number. L_R is the position of the corresponding pressure sensor in meters from the feed point [22].

$$Non-dimensional\ pulse\ frequency: Sr = \frac{f_P \bullet L_R}{v_F} \tag{6}$$

Transient analysis of the pressure signal was performed by Behera et al. [22] and Williams et al. [24,25]. They carried out conveying trials with fly ash and cement, which are both Geldart group C materials, in a DN50 conveying pipe with lengths of 130 m and 173 m. Three pressure sensors were installed and evaluated along the conveying line at 27 m, 90 m and 130 m from the feed point.

The course of the pulse slope ratio was evaluated along the conveying pipe. A clear course of the pulse slope ratio does not result. The change of the ratio along the pipe is increasing as well as decreasing,

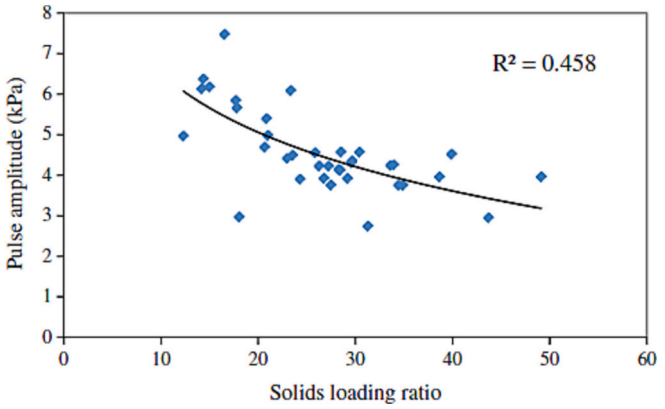

Fig. 5. Variation of pulse amplitude with solids loading ratio [22].

which is explained by Behera et al. [22] with the change of the flow mode along the pipe and the air holding capacity of the fly ash.

The pulsation frequency tends to decrease along the conveying line when the conveying starts as dense flow conveying. Like the pulse slope ratio, the course of the pulsation frequency is influenced by the flow mode and the air holding capacity according to [22].

The influence of the load on the transients is shown as an example in Fig. 5.

Fig. 5 shows that the pulse amplitude decreases with increase in the solids loading ratio. At low solids loading ratios, pulse amplitude is much higher due to higher pulse growth and vice versa.

Further investigation results are that the pulse slope ratio shows a decrease with increasing loading. If the SLR increases, the pulse amplitude difference falls, i.e. the height of the pressure fluctuation is reduced, which was justified with the aeration behaviour of the bulk material. The amplitude of the pressure increases along the conveying line depending on the bulk material and the flow mode, this is due to the gas expansion along the pipeline [25]. Deposits and dunes which will be accelerated have to be accelerated to higher velocity. This results into higher pressure drops and thus high pressure amplitudes. It was observed that the pulse amplitude decreases when the air mass flow is increased. The analysis with fly ash and alumina has shown an increase in pressure fluctuation with an increase in distance from the start of the pipeline. [24,25], i.e., that the pulsations increases along the conveying

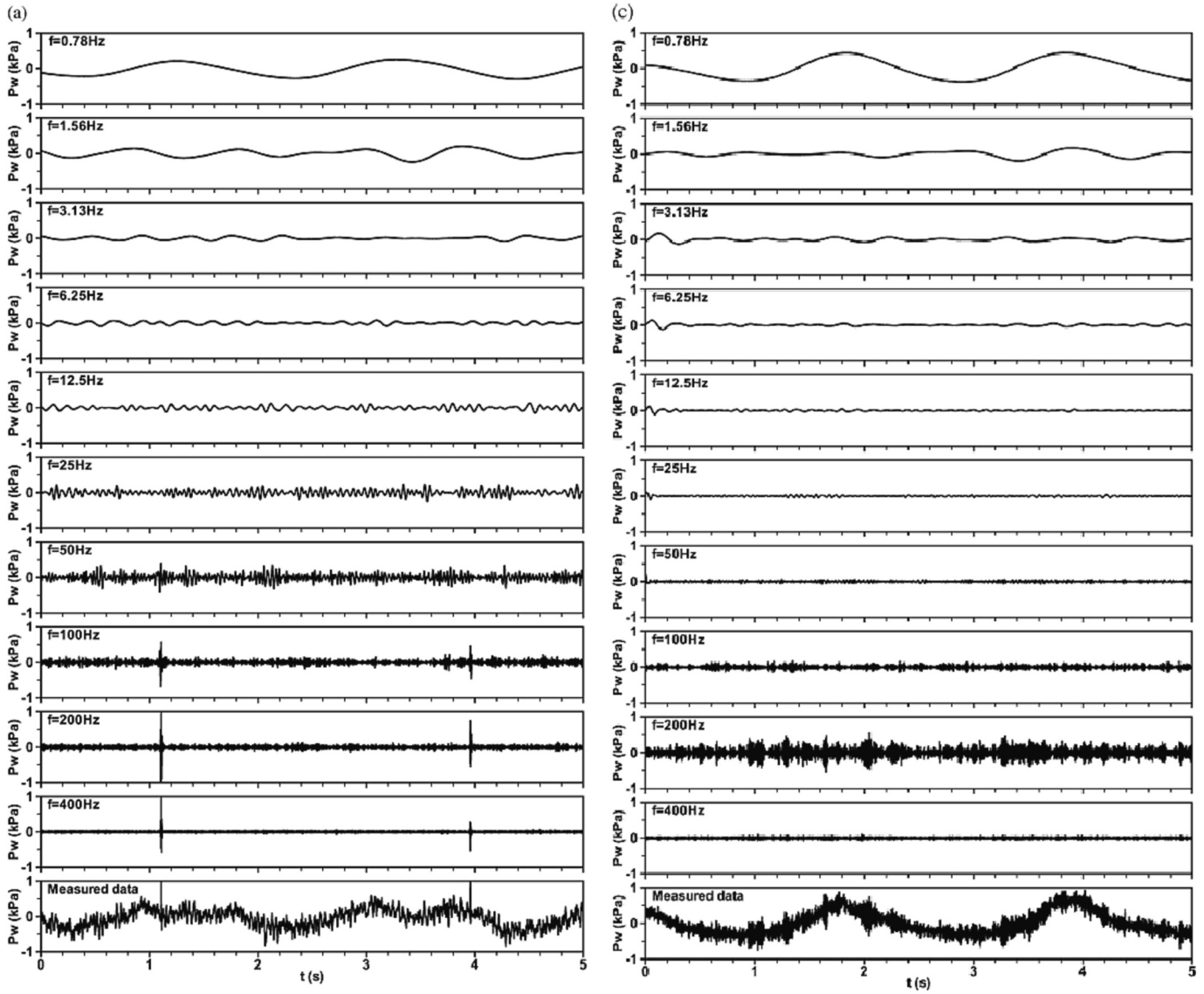

Fig. 6. Wavelet multi-resolution analysis of fluctuating pressure at air velocity of 10 m/s and 0.3 kg/s solids mass flow at locations of x = 2 m (left), x = 6 m (right) from feeding point [28].

pipeline, influenced only by the pipeline layout, such as bends. One reason could be that the re-acceleration of deposits along the conveying line due to the increasing air velocity and thus increasing relative velocity between air and deposit lead to higher acceleration pressure losses, which are measured in the form of pressure pulsations.

The results of the above shown transient analysis of the static pressure fluctuations with a Geldart group C material shows that with the help of transients, such as the rate of pressure increase, decrease, pulse time, pulse frequency, conclusions can be drawn about the flow condition and the aeration condition of the bulk material in the conveying pipeline. The strength of the pressure pulses appears to depend on the length of the pipe and the nature of the material. The solid mass flow rate showed only a small influence on the pulse structures. Bends influence the results, due to the rope formation. A turbulent flow will get smoothed due to the bend and the transients can change significant.

5.2. Frequency analysis

Frequency analysis is a tool for studying periodic signals such as pressure signals, as it allows the various frequency components of a signal to be identified and quantified to provide information about its characteristics.

If the Fourier transformation is used, which is a mathematical method for decomposing a signal into its individual frequency components, then a signal will be converted from the time domain to the frequency domain, allowing the various frequency components of the signal to be identified [90].

If the wavelet analysis will be used for frequency analysis, unlike Fourier analysis, which decomposes the signal into sine and cosine frequency components, wavelet analysis uses a basis function called a wavelet to divide the signal into different frequency ranges. Wavelet analysis can be useful in analysing signals where the frequency ranges vary or have sharp temporal changes, as it can capture these changes better than Fourier analysis [22].

5.3. Wavelet transformation / denoising

The origins of wavelet theory come from signal theory. It is a transformation of the frequency analysis of signals (time-dependent functions). This transformation was introduced because the classic methods for frequency analysis, i.e., the Fourier and the windowed Fourier transformation, have significant disadvantages in terms of signal theory. A major disadvantage of the Fourier transformation is that it insufficiently considers the local properties of a signal [26].

In the world of wavelets, the basic functions are called the scaling function and the mother wavelet. The wavelet function of the continuous wavelet transform is [26,28]:

$$W_k(\tau, s) = \frac{1}{\sqrt{|s|}} \int_{-\infty}^{+\infty} f(t)\, \psi(t) dt, \tag{7}$$

where f(t) ist the signal as a function of time (t) with the mother function / mother wavelet:

$$\psi(t) = \psi^* \left(\frac{t-\tau}{s}\right), \tag{8}$$

where s is the scaling parameter as the reciprocal of the frequency. It is used to set the width of the window function. τ is the time variable. If s and τ are defined in binary and discrete form, then the continuous wavelet transformation becomes the discrete wavelet transformation. Using the discrete wavelet transform has the advantages of more accurate and faster analysis. In this case the time variable τ becomes a and the scaling factor s becomes b. N is the length of the filter:

Table 2
Frequency bands of the wavelet analysis of plastic pellets in a swirling gas-solid flow [28–30,61,62,78].

Frequency band	Evaluation
0.5–1 Hz	Dune flow [28,29,61,62,78]
1.56–3.13 Hz	Periodic sliding clusters [78]
20–80 Hz	Heterogeneous suspension flow over dunes [29,61,62]
100–110 Hz	Dilute flow over dune flow [28–30,78]
120 Hz	Heterogeneous suspension flow [29,62]
20–200 Hz	Dilute flow over dune flow [28,29]
200 Hz	Only air flow [28–30]

$$W_a[a, b] = \frac{1}{\sqrt{b}} \sum_{i=0}^{N-1} f(t)\, \psi \left[\frac{t-a}{b}\right] \tag{9}$$

The wavelet transformation is also suitable for noise reduction, called denoising. The thresholding technique is used for this. Hard and soft thresholding are the most well-known variants. All small detail coefficients that can be traced back to the noise and fall below a specified threshold value ε are set to 0 and are not considered in the reconstruction. Very good results can be achieved with this method if the output signal has been oversampled [27].

Li et al. [28,29,61,62] carried out conveying tests with polyethylene pellets ($d_{s,50} = 3500$ µm, $\rho_p = 1210$ kg/m^3) in a conveying pipe with a diameter of 76 mm. Fig. 6 shows the wavelet decomposition of the pressure signal down to 10 iteration depths (10 frequency bands). The illustration on the left shows the breakdown of the conveyance with a SLR of 2, two meters from the feed point. Li et al. classifies the flow mode as dilute phase. The 200 Hz frequency (band 9) band shows the most intense deflections. For Li et al., the 200 Hz band is the characteristic band for dilute phase. The illustration on the right shows the decomposition of the conveyance six meters from the feed point. Li et al. classifies the conveyance as dune flow. The 0.78 Hz frequency in band 1 shows the most dominant deflections. 0.78 Hz corresponds to the frequency with which the dunes pass the pressure sensor. Here, too, the 200 Hz frequency band shows more intense deflections than the other bands. Li et al. interpret this as the dilute flow above the dunes.

Table 2 shows the summary of the authors [28–30,61,62,78] which indicated the flow pattern by the frequency peaks in the decomposed frequency bands. The tests were carried out with Geldart group D plastic granulates.

Mittel et al. [34] used wavelet analysis to assess the static pressure when conveying Geldart A particles. They presented their results by means of colour spectra. The colour intensity reflects the energy of the wavelet coefficients (also called scale coefficient), and the colour bar in each graph gives the energy values for the different colours. From the colour spectrum, they can determine that the conveyance at the beginning of the conveying line begins as a dune conveyance and becomes highly turbulent at the end of the line. They also observed that the magnitude of the maximum energy increases along the conveying pipeline, indicating an increase in the amplitude of the pressure fluctuations. Fig. 7 shows an example of the colour spectra for fly ash at a SLR of 63. At initial locations (i.e., at 6,7 m and 22,6 m from the feed point, maximum energy is concentrated in the upper region of the plot and corresponds to high scale coefficients (i.e., scale 50). Since higher scale coefficients describe the low frequency components of the signal, therefore it indicates that a signal is composed of large number of low frequency components, which might be due to reduced turbulence at the starting of pipe location and in turn indicates dune flow mechanism. While going from P2 (22,6 m from feed point) to P3 (75,3 m from feed point), colour intensity is reduced corresponding to higher scales (i.e., changes from dark red to light blue) and higher intensity shifts to lower scales (i.e., scale 20). Thus, parent signals contain comparatively higher frequency features as compared to the signal obtained at location P1. With further movement along the pipeline (i.e., from 75,3 m to 115 m

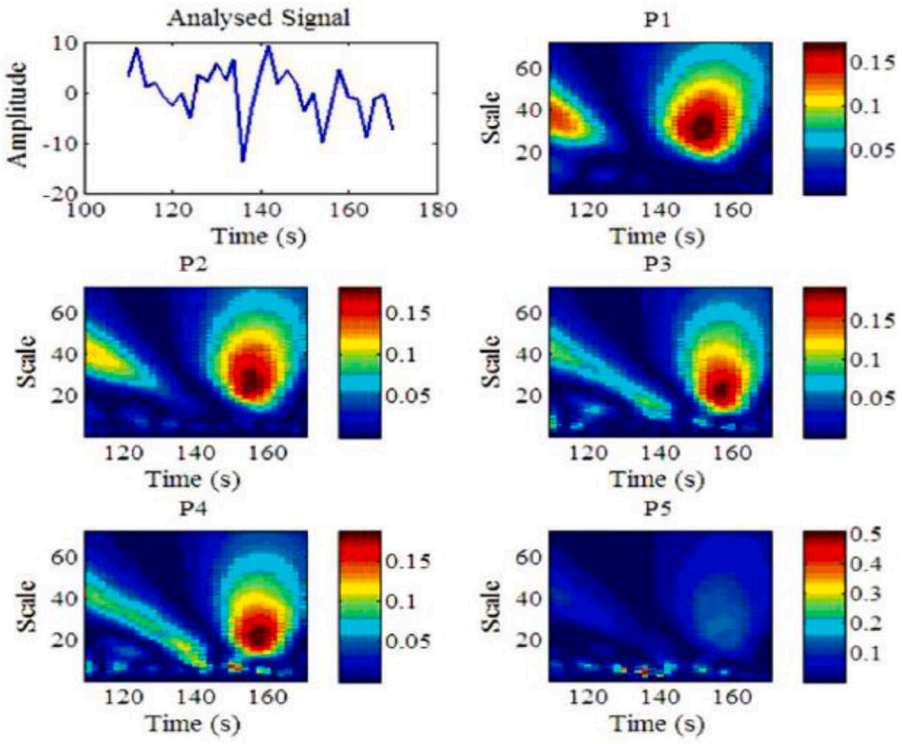

Fig. 7. Variation of energy distribution in different levels along the length (P1 to P5) for fly ash at a SLR of 63 [34].

from feed point) colour intensity almost diminishes at higher scales and multiple numbers of highly concentrated points are seen at lower scales (scale 10), which indicate the presence of large number of pressure fluctuations at different time instants in the signal [34].

5.4. Power spectral density (PSD)

The spectral analysis gives the spectral power density as a result. If it is applied to the pressure signals p of the pneumatic conveying, the power of a frequency range in the unit [Pa^2/Hz] is obtained. Plotted against the frequency shows the dominant frequencies that are generated, for example, by the feeding device, the pressure generator or by the conveyance.

An analogue signal p(t) is digitally sampled and is now dependent on the number of samples n. The pressure data series are divided into L segments with a length of N_S for each window-segment $x_i[n]$ and represented as follows [31]:

$$p[n] = p[n + iN_s] \tag{10}$$

$$with\ n = 1, 2, \ldots, N_S\ and\ i = 1, 2, \ldots (L-1)$$

In order to get the lowest variance from a fixed number of samples, it turns out to be optimal to overlap the window segments by half their length [32]. Each window-segment $x_i[n]$ is multiplied by a window function $w[n]$ [33]:

$$p_{w_i}[n] = p_i[n] \cdot w_i[n] \tag{11}$$

The Fourier transformation of the windowed signal can be expressed as follows [31]:

$$X_{w_i}[f] = \sum_{n=1}^{N_S} p_{w_i}[n] e^{-2\pi fn} \tag{12}$$

The corresponding power spectrum is the square of the absolute value of the amplitude and is according [31] for each segment *i*:

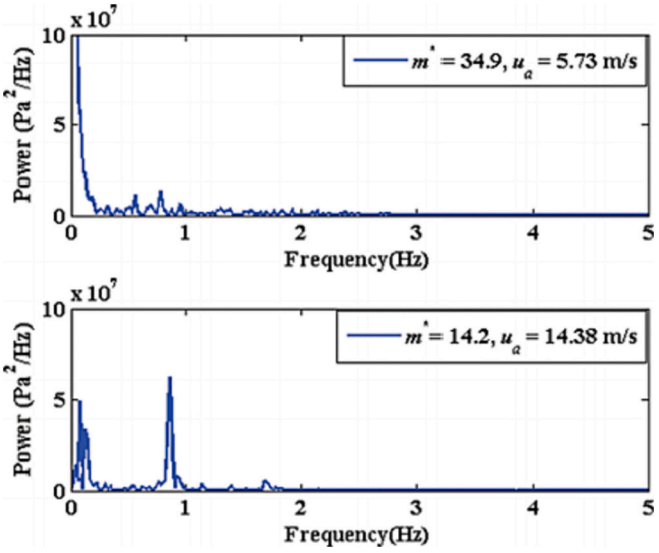

Fig. 8. PSD observations for dense and dilute-phase conveying of fly ash [36].

$$P_{xx}^{i}(f) = \frac{1}{N_S U} |X_{w_i}[f]|^2 \tag{13}$$

where U is a normalization factor related to the energy in the window function [31]:

$$U = \frac{1}{N_S} \sum_{n=1}^{N_S} w_i^2[n] \tag{14}$$

The average power spectrum is [31]:

$$P_{xx}(f) = \frac{1}{L} \sum_{i=1}^{L} P_{xx}^{i}(f) \tag{15}$$

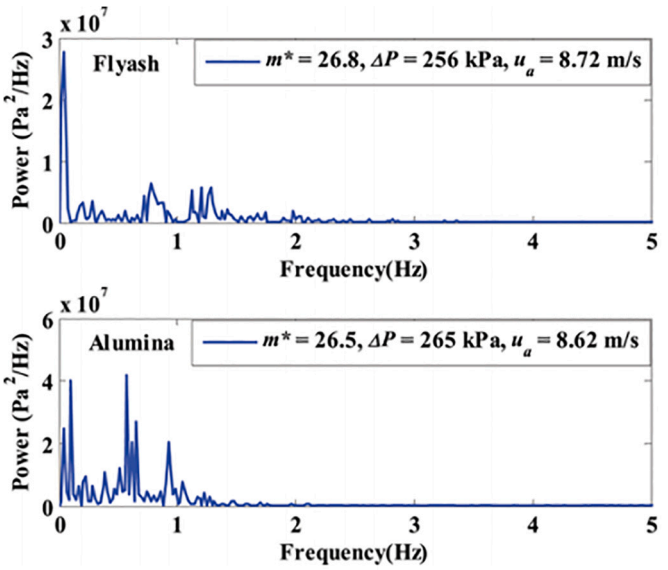

Fig. 9. Comparative PSD plot of fly ash and alumina under same flow conditions of conveying [36].

The result is a performance with unity $\left[\frac{Pa^2}{Hz}\right]$.

The PSD can also be used to distinguish between the periodic and chaotic nature of the flow process. A wide frequency band in the power spectrum indicates chaotic signal behaviour, while the periodic nature is reflected by clear dominant peaks in the frequency band [31].

In 1993, Dhodapkar and Klinzing [35] were the first to apply PSD to horizontal pneumatic conveyance. They measured the static and differential pressure on top and on the bottom of the pipe. According to Behera [36] the PSD of the signals from top and bottom transmitters is quite similar, so it is not possible to identify the different flow modes on the upper and lower sections of a pipeline. According to Cabrejos et al. [49] both measuring methods provide enough information to identify the different flow regimes by PSD analysis.

An example of a PSD plot is shown in Fig. 8 for fly ash ($d_{s,50} = 14.91$ µm, $\rho_p = 2096$ kg/m^3) with $\dot{m}$ as SLR and u_a as the gas velocity. The upper diagram shows dense phase conveyance, the lower one dilute phase conveyance. With dense phase conveying, the dominant frequency bands are close to the 0 Hz range. Dilute phase conveying analysis shows several dominant frequencies of smaller PSD altitude [36].

That the bulk solid has an influence in the PSD is shown in Fig. 9 for fly ash and alumina under similar flow conditions of SLR, pressure at the corresponding pressure sensor and superficial gas velocity. The order of magnitude of power is higher for alumina than that of fly ash [36]. The peak value of the PSD is at fly ash near 0 and for alumina between 0.6 and 1.0 for the same conditions (SLR, static pressure, velocity, pipe diameter).

For the following statements it must be considered that the operating conditions (piping configuration, bulk solids and flow data) on which the statements are based differs. The letters of the reference-exponent show the Geldart-group of the trials, on which the statement is based.

Dhodaqkar [35][A,B] established the following classification based on his measurement:

- Stratified flow - significant fluctuating components occur near 0 Hz with lower amplitudes.
- Dune - irregular fluctuations <4 Hz frequency.
- Air flow only - little pressure fluctuations with very low frequency of ~ 0.05 Hz.

Mittal et al. [34][A] found out that a single frequency component at 0.1 Hz indicates the periodic nature of the pressure signal, which might have occurred due to periodic rising of dunes near the pipeline entrance. [35][A,B] and Cong et al. [38][A] analysed, that, if small amounts of bulk material are added to the pure air flow (small SLR), the power spectrum is smoothed from over 100 Hz to <2 Hz. If the SLR is further increased, the power spectrum/pulsations increase again.

The results show, that independent on the Geldart classification the dominant frequencies shift from the dilute flow (comparatively high energy content) to the dense phase (comparatively low energy content, because the particle absorb the energy) towards 0 Hz [34-46[C,A], 47[D], 40[D], 51[D], 62[D]]. Cong [39][A] measured, that the peak of the PSD decreases with increasing pipe diameter. Increasing bulk solids mass flow of coarse particles increases the peak value of the PSD.

The PSD peak value depends on the flow condition, test rig set up and bulk solid. For fine bulk solids the peak of the PSD decreases with increasing air at the beginning of the conveying line. For the same measuring position, the dominant frequency shows no tendency with increasing air velocity, because of the influence of the flow pattern. Bends influences the data of PSD for pressure sensors close before and behind the bend, due to strand and rope formation. Usually, the frequency shifts in the direction of larger values.

At the beginning of the conveying pipe, the power spectrum is quite narrow, and a single dominant peak can be clearly seen in the spectrum. Along the pipeline and towards the flow direction, the spectrum becomes broader, and in addition to the single dominant frequency, other frequency components also appear in the spectrum [34,36]. At the same time, the power density of the signal increases from the inlet to the end of the pipeline.

5.5. Statistics

5.5.1. Standard deviation

The best-known measure of the spread of a distribution is the standard deviation $\tilde{s}$ or its square, the variance $\tilde{s}^2$. It measures the spread of the data around its mean. The variance of the pressure around its mean is [42]:

$$\tilde{s}^2 = \frac{1}{n}\left[(p_1 - \bar{p})^2 + \ldots + (p_n - \bar{p})^2\right] \tag{16}$$

The standard deviation is the root of the variance [42]:

$$\tilde{s} = \sqrt{\tilde{s}^2} \tag{17}$$

The standard deviation of the static and/or differential pressure signal was analysed by Dhodaqkar and Klinzing [35], the teams of Mittal and Mallick [43,45] and Cabrejos et al. [49]. It could be shown that the standard deviation is minimum dependent on the bulk solid, pipe diameter, pipeline configuration (length, bends), flow mode, mass flow (air, bulk solid) and SLR.

If the experiments from [35,43,45,49] are analysed, it becomes clear that after a bend measured pressures, have a tendency that the standard deviation falls in ¾ of the measured data, caused by the strand and rope formation. Also measuring points 10 m behind the bend shows this tendency.

In 2014, Mittal and Mallick [43] found that the standard deviation increases along the conveying line. They disproved this with further investigations in 2016. [34]

The standard deviation of both absolute and differential signals gives certain information about the flow regime of the gas-solids flow as it increases to a maximum value when saltation is approached [49]. Dhodaqkar and Klinzing [35] substantiates this statement for granules to the effect that the standard deviation only deviates strongly with the dune flow, whereas it decreases slightly with the stratified flow.

5.5.2. Root mean square (RMS)

In mathematics, the root mean square is a statistical measure of the

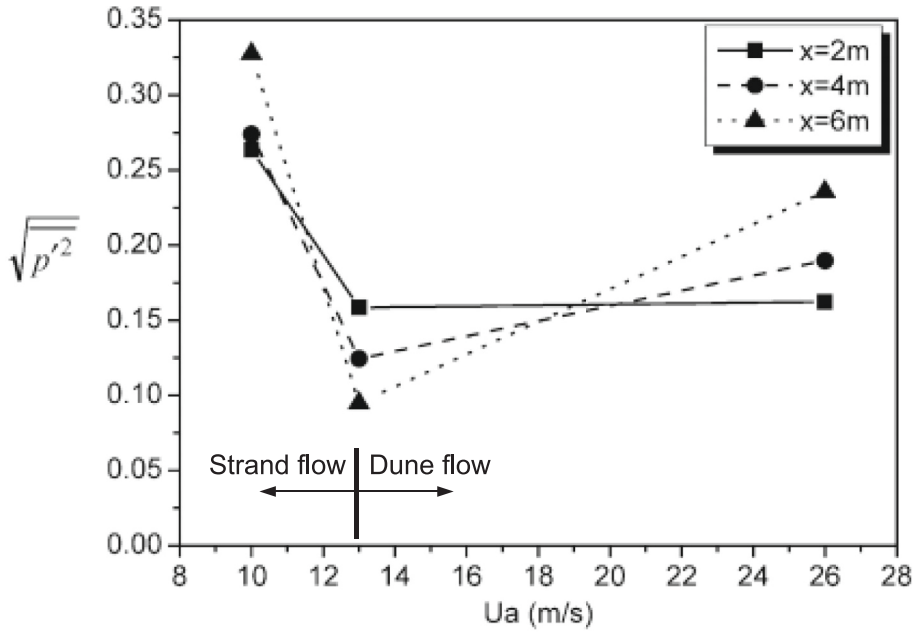

Fig. 10. RMS of the measured conveying line pressure p from with polyethylene pellets at a mass flow of 0.3 kg/s [28].

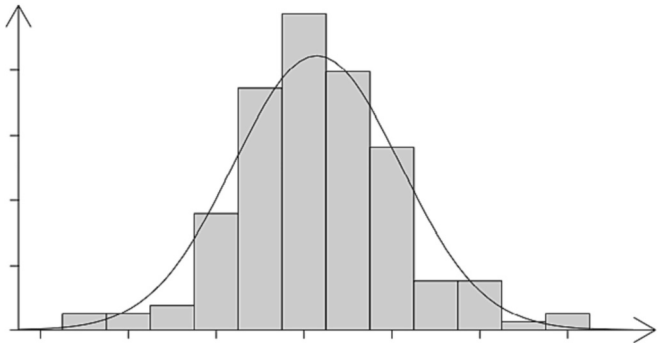

Fig. 11. Histogram and density function [42].

magnitude of a varying quantity. The square mean is a mean value in which large numbers are weighted more heavily than smaller numbers. In technology, the root mean square is of great importance for periodically changing quantities. The effective value, or root mean square is defined as follows [47]:

$$RMS = \sqrt{\overline{p^2}} = \sqrt{\frac{1}{n}\sum_{i=1}^{n} p_i^2} = \sqrt{\frac{p_1^2 + p_2^2 + \ldots + p_n^2}{n}} \tag{18}$$

Compared to the standard deviation, which accounts for the deviation of individual pressure signal from the mean, RMS accounts for the absolute magnitude of those pressure points as well.

Only Li [28] and Tsuji and Morikawa [48] analysed the pressure pulsation signal of a horizontal flow with the RMS. Both researchers used the static pressure signal of trials with plastic granulate. As an example, in Fig. 10, Li [28] shows the RMS of the conveying line pressure at 3 measuring points along the conveying line with 76 mm inner diameter for polyethylene pellets ($d_{s,50}$: 3.5 mm, ρ_p: 1210 kg/m^3). There is a kink point / minimum in the trends at an air velocity of 13 m/s. Both researchers showed, that for Geldart group D particles, the RMS increases sharply after a kink point with decreasing air velocity. For a Geldart group A/B material the RMS drops after passing this maximum. The reason is the change in flow mode from blowing dunes (mode B of Section 2) to strand flow and stratified flow (mode C and D of Section 2).

5.5.3. Probability density function (PDF)

Distributions describe the frequency of an occurring value x and are usually shown in so-called histograms (Fig. 11). To do this, classes are formed, and it is counted how often a value falls into a class. The probability density function PDF(x) is obtained by normalization of the continuous approximation of the histogram [27]. The following applies:

$$\int_{-\infty}^{+\infty} PDF(x)\mathrm{d}x = 1 \tag{19}$$

The probability density function describes the probability that a value x can assume in a distribution.

A so-called core density estimator is used to determine the PDF, since histograms can give a different impression due to different classifications. The equation for the core density estimator for approximating the PDF reads with b the bandwidth of a histogram window and n the number of samples [27]:

$$PDF(x_i) = \frac{1}{nb\sqrt{2\pi}} \sum_{i=1}^{n} e^{-\frac{1}{2}\left(\frac{x-x_i}{b}\right)^2} \tag{20}$$

The direct application of the PDF to the pressure signal found little use. Cabrejos et al. [49] noted about the absolute wall pressure of the transport of plastic granulate that the PDF changes from unimodal distribution for dilute flow and pulsating flow into a bimodal distribution for moving dunes and saltation back to a unimodal distribution for settled dunes.

Density curves are not only described by their position and scatter, but also characterized by the symmetry and *skewness* or *kurtosis* of the curve. These parameters always describe the deviation from the normal distribution. The index of skewness is the moment coefficient g_m, which is defined as follows [42]:

$$g_m = \frac{m_3}{\tilde{s}^3} \tag{21}$$

With:

$$m_3 = \frac{1}{n}\sum_{i=1}^{n}(x_i - \bar{x})^3, \tilde{s}^3 = \left(\sqrt{\frac{1}{n}\sum_{i=1}^{n}(x_i - \bar{x})^2}\right)^3 \tag{22a,b}$$

With:

$g_m = 0$ for symmetric distributions,
$g_m > 0$ for left-steep (right-skewed) distributions,
$g_m < 0$ for right-steep (left skewed) distributions.

Measures for the kurtosis are intended to characterize how heavily or weakly the central area and – related to this – the edge areas of the data are occupied. It should be noted that distributions with the same spread can have different kurtosis in the middle or different left and right ends in the edge areas. The kurtosis describes how flat or pointed a distribution is. The kurtosis number of a normal distribution is 3, so Fisher [42] normalized the kurtosis measure γ with "-3" and defined it as follows:

$$\gamma = \frac{m_4}{\tilde{s}^4} - 3 \tag{23}$$

With:

$$m_4 = \frac{1}{n}\sum_{i=1}^{n}(x_i - \bar{x})^4, \tilde{s}^4 = \left(\sqrt{\frac{1}{n}\sum_{i=1}^{n}(x_i - \bar{x})^2}\right)^4 \tag{24a,b}$$

With:
$\gamma = 0$ for normal distributions,
$\gamma > 0$ for sharper distributions,
$\gamma < 0$ for flatter distributions.

Tsuji and Morikawa [48] transported two different plastic pellets of Geldart group A/B and D. They evaluate their measurements for all Geldart groups, which were used, for the flow mode A and B (definition see Section 2). When the fluctuation follows the Gaussian probability distribution, the skewness and kurtosis factors have the values of 0 and 3, respectively. For bulk solid which is at the boundary of Geldart group A/B the dune flow has a positive skewness, the strand flow has a negative skewness. The Geldart group D bulk solid has a positive skewness in plug flow mode. For the kurtosis, all values are >0 for flow modes except A and B.

Cabrejos and Klinzing [49] could not determine any clear assignment of the skewness and kurtosis to the flow patterns when conveying coarse bulk solids.

5.6. Shannon entropy

The Shannon entropy, also called information entropy, describes the average amount of information contained in a signal. It comes from information theory and was developed by Claude E. Shannon in 1948. It is a measure of the uncertainty or disorder in the system and can be viewed analogously to entropy in thermodynamics [30]. It is defined as follows [50]:

$$H_s = -\sum_{i=1}^{n} P(x_i) log_b P(x_i), \tag{25}$$

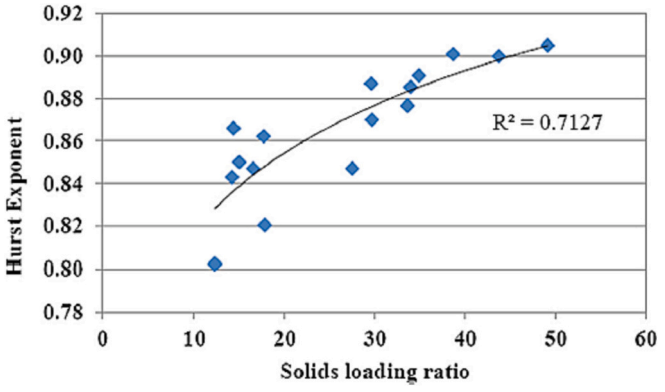

Fig. 12. Course of the Hurst exponent depending on the SLR for the pneumatic transport of fly ash [53].

where P is the probability of any value of x. The logarithmic base b is either 2, e or 10. The unit of P is with the b = 2 Bit, b = e Nat or b = 10 Hart [43].

Various investigations with fine bulk solids were carried out to determine the Shannon entropy using pressure measurements [43,45,46,50,53,79]. It turns out that the Shannon entropy depicts the flow conditions in the conveying line well. The Shannon entropy increases along the horizontal conveying line since the turbulence and thus particle contacts and particle-wall contacts increase for example due to increase in velocity. In the area of dense phase conveyance, the Shannon entropy is lower than in the area of dilute conveyance. Like the standard deviation, the Shannon entropy also changes after a bend. The Shannon entropy is also reduced because of the deceleration in the bend and the resulting reduction in turbulence. If the Shannon Entropy has a high or low level depends on the turbulence of the flow mode itself. The influence of the SLR or bulk solid mass flow is also linked to the flow mode. An increasing SLR or mass flow can increase and decrease the Shannon entropy. In case the increasing SLR or mass flow changes the flow mode from homogenous flow to strand flow, then the turbulence reduces, and the Shannon entropy reduces. If the SLR or mass flow changes from strand flow to dune flow the turbulence increases which lead to higher Shannon values.

It should be noted that the absolute value of the Shannon entropy depends on the amount of data, so attempts are only comparable when the same number of data is considered.

5.7. Rescaled range analysis / Hurst exponent

The rescaled range analysis was developed in 1951 by British hydrologist Harold Edwin Hurst to assess and forecast Nile water levels. The method should detect stability and near instability [51].

The Hurst exponent is calculated in six steps as follows [52]:

1) Calculation of the mean $\bar{p}$
2) Calculation of the linear deviation from the mean:

$$y_i = p_i - \bar{p} \tag{26}$$

3) Calculation of the cumulative deviation from the deviation of the mean:

$$z_i = y_i + y_{i+1} \tag{27}$$

4) Determining the rescaled range:

$$R = max(z_i) – min(z_i) \tag{28}$$

5) Calculation of the standard deviation $\tilde{s}$ according to Eq. (17).
6) The Hurst exponent is then defined as follows (with n as the time window of the measurement interval):

$$\frac{R}{\tilde{S}} \propto n^{H_x} \rightarrow H_x = \frac{ln\frac{R}{\tilde{S}}}{lnn} \tag{29}$$

The exponent can be divided into 3 areas, which are generally interpreted as follows:

$H_x < 0.5$	Indicates a time series with long-term alternation between high and low values in adjacent pairs, meaning that a single high value is likely to be followed by a low value and that the value will then tend to be high again, with this tendency to switching between high and low values long into the future.
$H_x = 0.5$	Shows that the values will not show any long-term correlation.
$H_x > 0.5$	Indicates a time series with long-term positive autocorrelation, which means both that a high value in the series is likely to be followed by another high value, and that values will tend to be high as well long into the future.

Table 3
Summary of Hurst exponent evaluation.

Hurst exponent	Evaluation
< 0.08	Unstable flow [51]*
0.1 … 0.3	Stable flow** [51]
0.35 … 0.5	Only gas flow [49]
0.35 … 1.15	Conveying with bulk solid [49]
< 0.40	Only gas flow [37,40]
0.40 … 0.80	Dilute flow, strand flow, unstable flow* [49]
0.40 … 0.99	Conveying with bulk solid [50]
0.57 … 0.92	Conveying with bulk solid [37,40]
0.60 … 1.15	Flow below saltation velocity [49]
> 0.74	Flow left of the minimum point of pressure drop [38]
0.70 … 0.90	Conveying with bulk solid [38]
0.80 … 0.91	Conveying with bulk solid [37,40]
0.80 … 1.10	Dune flow [49]
< 0.84	Dilute flow [37,40]

Various authors [37,38,40,45,49,51,53] have applied the rescaled area analysis to pneumatic conveying by using absolute or differential pressure signals, with a variety of statements that must be considered very much in relation to the respective test rig.

The final statements are that in a pneumatic conveying system the Hurst Exponent decreases along the direction of flow in case the flow mode changes also [40,43,53,59], what implies that there is an increase in degree of complexity of flow mechanism (or turbulence), comparable to the Shannon entropy and that the Hurst exponent increases after passing a bend [43].

[37,40,46,53] found that the Hurst exponent also increases with increasing SLR, which is attributed to damping of the flow and thus reduction of flow turbulence.

As an example, the course of the Hurst exponent is shown using fly ash conveyance as a function of the SLR, see Fig. 12. Shijo and Behera [53] transported fly ash ($d_{s,50} = 14.91$ µm, $\rho_p = 2096$ kg/m^3) through a 173 m long conveying line with a pipe diameter of 53 mm, measuring the static pressure of the system. It turns out that the Hurst exponent increases as the SLR increases. That the Hurst exponent increases with increasing SLR could not be confirmed by all authors, because an increasing SLR could lead to a change of flow mode, and then also a change of the Hurst exponent into the opposite direction is possible. Since not only the SLR influences the Hurst exponent, but also the change flow mode.

The results from Table 3 and Fig. 13 show that the Hurst exponent is not a good method to compare conveying systems with each other. The ranges of the absolute values overlap considerably, so that no clear assignment of a Hurst exponent to a flow mode is possible. Since a small Hurst exponent means a large disorder / turbulence, one can recognize the change of the flow mode in a system based on the Hurst exponent, which is again comparable with the Shannon entropy.

Fig. 13 show the classification of the results to the flow modes from Table 3. *Unstable flow is a mode of conveying for coarse particles where the system is in equilibrium between plug and strand flow [51]. **flow occurs near the pressure drop minimum and is valid for coarse particles [51].

5.8. Phase space diagram

Phase space diagrams are useful to represent chaotic systems or deterministic dynamic systems that are extremely sensitive to disturbances in their initial conditions. It is possible to construct the 2-dimensional state space plot by means of only one characteristic variable by using the method of delay coordinates [54]. The values of the variable at different time delays {0, Δt, 2Δt, …, (d − 1)Δt} are used as coordinate values in the embedding space. 2-dimensional phase space diagrams have been constructed using the method of delays [55], which involves plotting original time series X(t) versus its delayed versions, i.e. X(t + τ), where τ is the delay time to collect one data point.

The normalized pressure at time t and its time derivate (dp/dt) at the same time, (dp/dt) is defined as follows [40]:

$$\frac{dp}{dt} = \frac{P(t+\Delta t) - P(t)}{\Delta t} \tag{30}$$

The phase space diagram is represented by the normalized value of pressure drop per unit length at a certain time (t) versus the normalized value of pressure drop per unit length at (t + dt), where (dt) represented the time step to collect one data point.

Selection of optimum value of delay time is important for phase space construction. If the selected time lag is too short, then there are chances that it would be influenced by noise, on the other hand if too

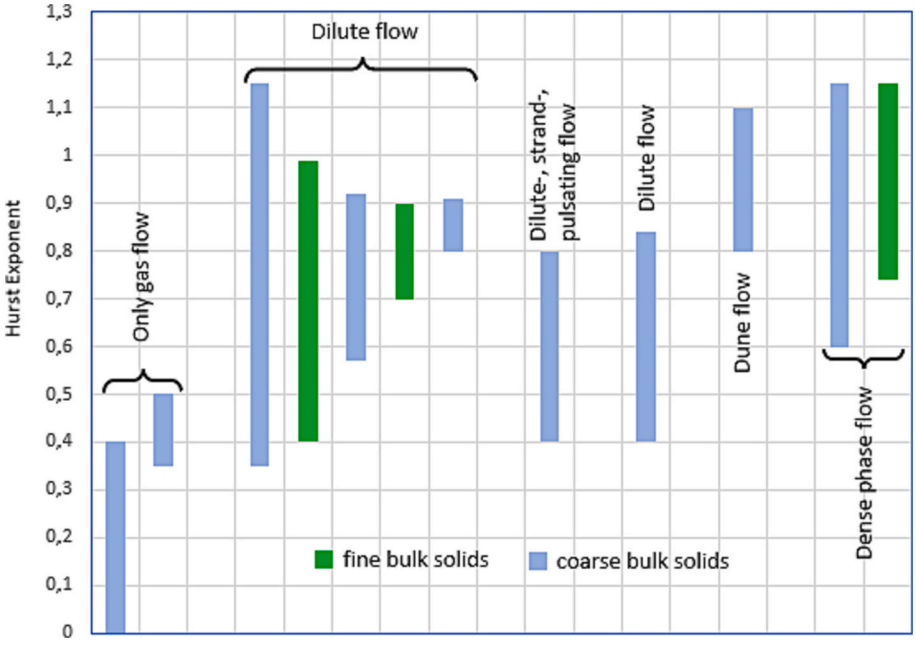

Fig. 13. Classification of flow patterns in horizontal pneumatic conveying using the Hurst exponent of pressure signals.

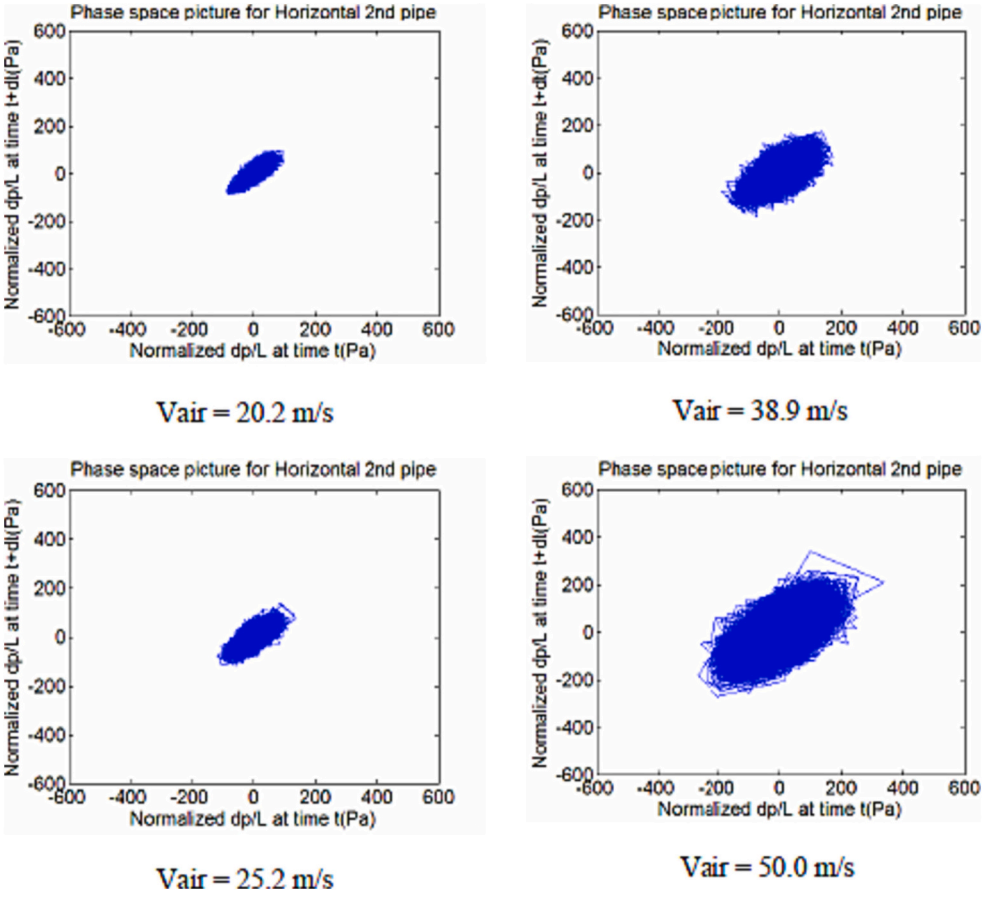

Fig. 14. Phase space diagram at lower horizontal section (gas only), with different air velocities [40].

long delay time is chosen, then the phase space attractor would not reveal the local flow characteristics. The optimum value of delay time is selected as the first minimum of the mutual information function [52].

Cabrejos [49,56] was in 1994 one of the first, who uses the phase diagram to judge about a pressure signal. Further investigations were carried out by [37,40,46,53]. Fig. 14 show as an example phase space diagrams from [40] for a horizontal pipe section, with air at different gas velocities. The diagrams shows that the area of the phase space diagram increases with increasing air velocity, because the turbulence increases.

Independent on the pressure measuring type (static pressure or differential pressure) the type of pulsation can be deduced from the geometric position of the data in the phase space diagram. The longer the horizontal length of the graph, the greater the pressure fluctuations. The longer the vertical height the faster the pressure fluctuations. An increase in the area means an increase in the turbulence in the conveying line, caused by e.g., higher fluid velocities or by the transition from dense flow conveying to dilute phase conveying, as can happen along a conveying line. However, the geometry of the diagram and its changes during conveying can only provide qualitative statements on turbulence and pulsation. It also follows that the influence of the loading allows to increase or decrease the diagram area, depending on whether the feeding of bulk material increases or decreases the turbulence. As with all previous evaluation methods, the measurement after a bend leads to a change in the direction of turbulence reduction. The phase space plots indicate that there is no specific range in values for size or area of the attractor for a dense or dilute mode of flow.

6. Conclusions

The previous scientific work evaluated the pressure signal using statistical analyses such as PSD, RMS, PDF, standard deviation (SD), root means square or the skewness or kurtosis. Also, non-statistical methods like wavelet analysis, transient parameter analysis, Shannon entropy, rescaled range analysis or the phase space diagram were used. Mainly qualitative and partially quantitative relationships to flow patterns were found.

In summary, turbulence is the key factor influencing the analysis methods. The standard deviation and the transients show the direct character of the pressure signal. Except for the phase space diagram, quantitative results are obtained which, however, have little significance on their own. In principle, the tendency of the measurement methods can be shown as a function of the turbulence as follows, if the turbulence increases, then:

- the pressure pulsations increase,
- the standard deviation of the pressure signal increases,
- the Shannon Entropy increases,
- the Hurst Exponent decreases,
- the area of the phase space diagram increases,
- the dominate frequency of the wavelet analysis increases,
- the power spectral density increases.

The turbulence is a function of the relevant process parameters like for example air velocity, particle velocity, SLR, mass flow, bulk solids data, pipe diameter and pipe configuration. All these data results into a plant specific flow mode. The turbulence can be linked to the flow, for example acc. [80] mode of Section 2 as follows:

- High turbulence flow modes are: Dilute flow, cluster flow, unstable dune flow (mode A, B, E)
- Medium and low turbulence flow modes are: Strand flow, stratified flow (mode C, D), plug flow (mode F)

Table 4
Geldart groups which were used for the analysis method acc. [22–25,28–30,34–43,45,48–51,55,56,61,62,78,79].

Analysis method	Geldart group			
	C	A	B	D
Transients	X	–	–	–
Wavelet	–	X	–	X
Power spectral density	X	X	X	X
Standard deviation	X	X	X	X
Root mean square	–	–	–	X
Probability density function	–	–	X	X
Shannon Entropy	X	X	–	–
Hurst Exponent	X	X	X	X
Phase space diagram	X	X	X	X

Table 4 shown the analysed bulk solids classified into the Geldart group and linked to the analysis method.

However, the results obtained so far still show room for further investigations, so the influence of the pipe diameter on the pulsations has hardly been investigated, and the application of the root mean square and the probability density function to the pressure signal has only been used to a limited extent. Depending on the Geldart group or the flow mode, how does the pressure signal behave below the minimum pressure loss in the direction of the minimum conveying velocity? Can an analysis method be used to detect blockages before they occur? Are there other transients that describe the flow modes, the minimum pressure drops, the minimum conveying gas velocity, such as the ratio of the pressure rise time to the pressure drop time of a pulsation, or the ratio of the absolute pressure increase to the absolute pressure drop of a pulsation. What about the absolute pressure in the conveying line, how does it influence the pressure signal? The higher density results into a higher impulse onto the particles and it could result in a change in flow mode. So further investigations must be carried out, to get a clear and deep understanding of pressure pulsation in horizontal pneumatic conveying lines.

CRediT authorship contribution statement

M. Dikty: Writing – review & editing, Writing – original draft, Validation, Supervision, Project administration, Investigation.

Declaration of competing interest

The authors declare that they have no known competing financial interests or personal relationships that could have appeared to influence the work reported in this paper.

Data availability

No data was used for the research described in the article.

References

[1] R.D. Marcus, F. Rizk, S.J. Meijers, Solids handling, in: Ullmann's Encyclopedia of Industrial Chemistry, 7th edition, Wiley-VCH, Weinheim, 2002.
[2] P. Hilgraf, Pneumatische Förderung, Springer, Berlin, 2019.
[3] P.W. Wypych, Effect of rotary valve leakage on pneumatic conveying performance, Part. Sci. Technol. 26 (2008) 257–272.
[4] M. Dikty, A. Akdag, P. Kühn, Successful operation of ceramic rotary valves at Karsdorf cement plants, Cement International 3 (2019) 46–53.
[5] G.E. Klinkzing, F. Rizk, R. Marcus, L.S. Leung, Pneumatic Conveying of Solids, Springer, 2010.
[6] D. Mills, M.G. Jones, V.K. Agarwal, Handbook of Pneumatic Conveying Engineering, Marcel Dekker, 2004.
[7] P. Hilgraf, J. Paepcke, Introducing bulk materials into pneumatic conveying lines with screw feeders, ZKG Int. 7 (1993) 368–375.
[8] M. Dikty, Dust pumps according to ATEX 95, Bulk Solids Handl. 26 (6) (2006) 420–426.
[9] K. Schneider, Einsatz des Gas-Feststoff-Injektors als Einschleusorgan bei der pneumatischen Förderung von Schüttgütern, SCHÜTTGUT 2 (2) (1996) 217–224.
[10] M. Dikty, P. Schwei, Decision matrix for bulk solids transport, ZKG Int. 7 (60) (2007) 56–66.
[11] M.G. Jones, K.C. Williams, Predicting the mode of flow in pneumatic conveying systems - a review, Particuology 6 (2008) 289–300.
[12] E. Muschelknautz, Theoretische und experimentelle Untersuchungen über die Druckverluste pneumatischer Förderleitungen unter besonderer Berücksichtigung des Einflusses von Gutreibung und Gutgewicht, VDI-Forschungsheft 476 (1959).
[13] F. Ebert, Verfahrenstechnik Mainz 8 (2) (1974) 36–41.
[14] C.T. Crowe, J.D. Schwarzkopf, M. Sommerfeld, Y. Tsuji, Multiphase Flows with Droplets and Particles, 2nd edition, CRC Press, 2011.
[15] M. Bohnet, Experimentelle und theoretische Untersuchungen über das Absetzen, das Aufwirbeln und den Transport feiner Staubteilchen in pneumatischen Förderleitungen, VDI-Forschungsheft 507 (1965).
[16] E. Muschelknautz, W. Krambrock, Vereinfachte Berechnung horizontaler pneumatischer Förderleitungen bei hoher Gutbeladung mit feinkörnigen Produkten, Chem.-Ing.-Tech. 41 (21) (1969) 1164–1172.
[17] K.E. Wirth, Die Grundlagen der pneumatischen Förderung, Chem.-Ing.-Tech. 55 (2) (1983) 110–122.
[18] E. Rabinovich, H. Kalman, Boundary saltation and minimum pressure velocities in particle-gas systems, Powder Technol. 185 (2008) 67–79.
[19] L.M. Gomes, A. Mesquita, On the prediction of pickup and saltation velocities in pneumatic conveying, Braz. J. Chem. Eng. 31 (1) (2014) 35–46.
[20] A. Biobaku, W. Schmitz, R. Naidoo, Evaluation and comparison of saltation velocity correlations in the context of pulverized fuel transport, Energy 181 (2019) 694–708.
[21] M. Dikty, 190014 – conveying trials with lime stone, Krauschwitz (2019) (unpublished, Internal R&D report).
[22] N. Behera, V.K. Agarwal, M.G. Jones, K.C. Williams, Transient parameter analysis of fluidized dense phase conveying, Powder Technol. 217 (2012) 261–268.
[23] W. Chen, K.C. Williams, I. Jabs, M.G. Jones, A qualitative study on the pulsatile flow phenomenon in a dense fly ash pneumatic conveyor, Particuology 17 (2014) 81–91.
[24] C.K. Williams, M.G. Jones, A.A. Cenna, Characterization of the gas pulse frequency, amplitude and velocity in non-steady dense phase pneumatic conveying of powders, Particuology 6 (2008) 301–306.
[25] K.C. Williams, M.G. Jones, Y. Yadav, Pressure fluctuations in dense phase pneumatic conveying of powders, Partec (2007).
[26] A.K. Louis, P. Maaß, A. Rieder, Wavelets – Theorie und Anwendungen, Teubner Stuttgart, 1988.
[27] P. Baumm, Beurteilung von Signalverarbeitungsmethoden an pulsierenden pneumatischen Förderungen, Bachelor-Thesis, Hamburg, 2020.
[28] H. Li, Application of the wavelet multi-resolution analysis to pressure fluctuations of gas-solid two-phase flow in a horizontal pipe, Powder Technol. 125 (2002) 61–730.
[29] H. Li, Y. Tomita, Identification of flow pattern in horizontal pneumatic conveying by wavelet analysis, in: Proceedings of the 2nd International Conference on Material Handling, 1997, pp. 584–588.
[30] R. Tong, Wavelet analysis of pressure fluctuation in gas-solid two-phase flow in a horizontal pipe, in: 2011 2nd International Conference on Mechanic Automation and Control Engineering, 2011, pp. 932–935.
[31] M. Werner, Digitale Signalverarbeitung mit MATLAB, Vieweg, 2006.
[32] J. Xiang, Q. Li, Z. Tan, Y. Zhang, Characterization of the flow in a gas-solid bubbling fluidized bed by pressure fluctuation, Chem. Eng. Sci. 174 (2017) 93–103.
[33] W.T. Vetterling, S.A. Teukolsky, W.H. Press, B.P. Flannery, Numerical Recipes in C: The Art of Scientific Computing, Cambridge University Press, 1999.
[34] A. Mittal, S.S. Mallick, P.W. Wypych, An investigation into the transition of flow mechanism during fluidized dense-phase pneumatic conveying of fine powders, Part. Sci. Technol. 34 (1) (2016) 23–32.
[35] S.V. Dhodapkar, G.E. Klinzing, Pressure fluctuations in pneumatic conveying systems, Powder Technol. 74 (2) (1993) 179–195.
[36] N. Behera, V.K. Agarwal, M. Jones, K.C. Williams, Power spectral density analysis of pressure fluctuation in pneumatic conveying of powders, Part. Sci. Technol. 33 (5) (2015) 510–516.
[37] J.B. Pahk, G.E. Klinzing, Assessing flow regimes from pressure fluctuations in pneumatic conveying of polymer pellets, Part. Sci. Technol. 26 (2008) 247–256.
[38] X. Cong, X. Guo, X. Gong, H. Lu, W. Dong, Experimental research of flow patterns and pressure signals in horizontal dense phase pneumatic conveying of pulverized coal, Powder Technol. 208 (2011) 600–609.
[39] X. Cong, X. Guo, X. Gong, H. Lu, W. Dong, K. Liu, X. Sun, K. Xie, Flow patterns of pulverized coal pneumatic conveying and time-series analysis of pressure fluctuations, Chem. Eng. Sci. 101 (2013) 303–314.
[40] J.B. Pahk, Experimental Study of Pressure Fluctuation in Pneumatic Conveying by Various Methods of Analysis, PhD, Pittsburgh, 2006.
[41] B.J. Azzopardi, K. Jackson, J.P. Robinson, R. Kaji, M. Byars, A. Hunt, Fluctuations in dense phase pneumatic conveying of pulverized coal measured using electrical capacitance tomography, Chem. Eng. Sci. 63 (2008) 2548–2558.
[42] L. Fahrmeir, C. Heumann, R. Künstler, I. Pigeot, G. Tutz, Statistik: Der Weg zur Datenanalyse, Springer-Verlag, 2016.
[43] A. Mittal, S.S. Mallick, P.W. Wypych, An investigation into flow mode transition and pressure fluctuations for fluidiuzed dense-phase pneumatic conveying of fine powders, Particuology 16 (2014) 187–195.
[44] P. Hilgraf, J. Bartusch, Fluctuations in the mass flow of solids in pneumatic conveying lines, Cement International 6 (17) (2019) 37–45.

[45] A. Goel, A. Mittal, S.S. Mallick, A. Sharma, Experimental investigation into transient pressure pulses during pneumatic conveying of fine powders using Shannon entropy, Particuology 29 (2016) 143–153.
[46] A. Mittal, S.S. Mallick, P.W. Wypych, An investigation into pressure fluctuations for fluidized dense-phase pneumatic transport of fine powders, Powder Technol. 277 (2015) 163–170.
[47] J.F. Kenney, Mathematics of Statistics, D. Van Nostrand, 1939.
[48] Y. Tsuji, Y. Morikawa, Flow pattern and pressure fluctuation in air-solid two-phase flow in a pipe at low air velocities, Int. J. Multiphase Flow 8 (1982) 329–341.
[49] F.J. Cabrejos, G.E. Klinzing, Characterization of dilute gas-solids flows using the rescaled range analysis, Powder Technol. 84 (1995) 139–156.
[50] Y. Alkassar, V.K. Agarwal, R.K. Pandey, N. Behera, Experimental study and Shannon entropy analysis of pressure fluctuations and flow mode transition in fluidized dense phase pneumatic conveying of fly ash, Particuology 49 (2020) 169–178.
[51] G.A. Jama, G.E. Klinzing, F. Rizk, Analysis of unstable behaviour of pneumatic conveying systems, Part. Sci. Technol. 17 (1–2) (1999) 43–68.
[52] W.L. Li, W.Q. Zhong, B.S. Jin, R. Xiao, T.T. He, Flow regime identification in a three-phase bubble column based on statistical, Hurst, Hilbert–Huang transform and Shannon entropy analysis, Chem. Eng. Sci. 102 (2013) 474–485.
[53] J.S. Shijo, N. Behera, Transient parameter analysis of pneumatic conveying of fine particles for predicting the change of mode of flow, Particuology 32 (2017) 82–88.
[54] T.J. Lin, R.C. Juang, Y.C. Chen, C.C. Chen, Prediction of flow transitions in bubble columns by chaotic time series analysis of pressure fluctuation signals, Chem. Eng. Sci. 56 (2001) 1057–1065.
[55] F. Takens, Detecting strange attractors in turbulence, Lect. Notes Math. 898 (1981) 103.
[56] F.J. Cabrejos, Experimental Investigation on the Fully Developed Pipe Flow of Dilute Gas – Solids Suspensions vol. 210, University of Pittsburgh Press, Pittsburgh, 1994, pp. 157–208.
[57] F. Yan, A. Rinoshika, Particle fluctuation velocity of a horizontal self-excited pneumatic conveying near the minimum pressure drop, Powder Technol. 241 (2013) 115–125.
[58] F. Yan, A. Rinoshika, W. Tang, R. Zhu, Experimental analysis on particle fluctuation velocity in a horizontal air-solid two-phase pipe flow having a dune model, Part. Sci. Technol. 37 (2) (2019) 182–189.
[59] Y. Zheng, A. Rinoshika, Wavelet multi-resolution analysis on particle dynamics in a horizontal pneumatic conveying, Adv. Powder Technol. 29 (10) (2018) 2404–2415.
[60] A. Rinoshika, Y. Zheng, F. Yan, Wavelet analysis on particle dynamics in a horizontal air-solid two-phase pipe flow at low air velocity, Exp. Fluids 52 (2012) 137–149.
[61] H. Li, Multiresolution analysis of pressure fluctuation in horizontal swirling flow pneumatic conveying using wavelets, Adv. Powder Technol. 11 (4) (2000) 423–438.
[62] H. Li, Y. Tomita, Characterization of pressure fluctuation in swirling gas-solid two-phase flow in a horizontal pipe, Adv. Powder Technol. 12 (2) (2001) 169–185.
[63] A.J. Jaworski, T. Dyakowski, Investigations of flow instabilities within the dense pneumatic conveying system, Powder Technol. 125 (2002) 279–291.
[64] T. Dyakowski, L.F.C. Jeanmeure, A.J. Jaworski, Applications of electrical tomography for gas–solids and liquid–solids flows—a review, Powder Technol. 112 (2000) 174–192.
[65] K.C. Williams, M. Jones, B. Singh, Electrical capacitance tomography of dense-phase pneumatic conveying of fly ash, in: Bulk Europe Conference, Prague, 2008.
[66] C. Xu, C. Liang, B. Zhou, S. Wang, HHT analysis of electrostatic fluctuation signals in dense-phase pneumatic conveying of pulverized coal at high pressure, Chem. Eng. Sci. 65 (2010) 1334–1344.
[67] W. Pu, C. Thao, Y. Xiong, C. Liang, X. Chen, Numerical simulation on dense phase pneumatic conveying of pulverized coal in horizontal pipe at high pressure, Chem. Eng. Sci. 65 (2010) 2500–2512.
[68] W. Chen, K.C. Williams, M.G. Jones, Decomposition and statistical analysis of bulk density levels of dense phase fly ash powder flow within a pneumatic conveyor, Adv. Mater. Res. 239-242 (2011) 3323–3326.
[69] F. Fu, C. Xu, S. Wang, Flow characterization of high-pressure dense-phase pneumatic conveying of coal powder using multi-scale signal analysis, Particuology 36C (2018) 149–157.
[70] A. Rinoshika, Y. Zheng, F. Yan, Multi-scale analysis on particle fluctuation velocity near the minimum pressure drop in a horizontal pneumatic conveying, Chem. Eng. Sci. 72 (2012) 94–107.
[71] Y. Zheng, A. Rinoshika, Multi-scale particle dynamics of low air velocity in a horizontal self, excited gas-solid two-phase pipe flow, Int. J. Multiphase Flow 53 (2013) 114–123.
[72] Y. Zheng, A. Rinoshika, Analysis of particle dynamics in a horizontal pneumatic conveying of the minimum pressure drop based on POD and wavelet transform, Powder Technol. 320 (2017) 726–738.
[73] X. Li, F. Yan, P. Tu, Y. Chen, R. Zheng Zhu, Particle dynamics analysis in bend in a horizontal-vertical pneumatic conveying system with oscillatory flow, Adv. Powder Technol. 32 (2021) 637–645.
[74] F. Yan, A. Rinoshika, Application of high-speed PIV and image processing to measuring particle velocity and concentration in a horizontal pneumatic conveying with dune model, Powder Technol. 208 (2011) 158–165.
[75] Y. Tsuji, Y. Morikawa, LDV measurements in an air-solid two-phase flow in a horizontal pipe, J. Fluid Mech. 120 (1982) 385–409.
[76] K.H. Henthorn, K. Park, J.S. Curtis, Measurement and prediction of pressure drop in pneumatic conveying: effect of particle characteristics, mass loading, and Reynolds number, Ind. Eng. Chem. Res. 44 (2005) 5090–5098.
[77] T. Dyakowski, S.D. Luke, K.L. Ostrowski, R.A. Williams, On-line monitoring of dense phase flow using real time dielectric imaging, Powder Technol. 104 (1999) 285–295.
[78] A. Rinoshika, M. Takei, Y. Tomita, Y. Saito, K. Horii, Wavelet multi-resolution cross-correlation analysis of swirling gas-solid flow in a horizontal pipe, Part. Sci. Technol. 22 (2004) 107–118.
[79] C. Liang, C. Zhao, Y. Chen, W. Pu, P. Lu, C. Fan, Flow characteristics and Shannon entropy analysis of dense-phase pneumatic conveying of pulverized coal with variable moisture content at high pressure, Chem. Eng. Technol. 30 (7) (2007) 926–931.
[80] A. Patankar, A. Makawana, M. Bose, Dune Formation in Horizontal Pneumatic Conveying System. Fluid Mechanics and Fluid Power, Springer, India, 2017.
[81] M. Weber, Strömungsfördertechnik, Krausskopf-Verlag, 1973.
[82] O. Molerus, Fluid-Feststoff-Strömungen, Springer, 1982.
[83] A. Lippert, Die Staub-Luft-Förderung von Pulvern und Schüttgütern mit hohen Gutkonzentrationen im Gasstrom, PhD, Leverkusen, 1965.
[84] G. Welschof, Pneumatische Förderung bei großen Fördergutkonzentrationen, VDI-492/28, Düsseldorf, 1962.
[85] F.A. Zenz, D.F. Othmer, Fluidization and Fluid-Particle Systems, Reinhold Publishing Corporation, New York, 1960.
[86] N. Behera, V.K. Agarwal, M.G. Jones, K.C. Williams, CFD modelling and analysis of dense phase pneumatic conveying of fine particles including particle size distribution, Powder Technol. 244 (2013) 30–37.
[87] F.J. Cabrejos, G.E. Klinzing, Minimum conveying velocity in horizontal pneumatic transport and the pickup and saltation mechanisms of solid particles, Bulk Solids online 14 (3) (1994) 541–550.
[88] K.-E. Wirth, O. Molerus, Stopfgrenze und Druckverlust bei der horizontalen pneumatischen Strähnenförderung in nichtkreisrunden Rohrquerschnitten, Chem.-Ing.-Techn. 57/6 (1985).
[89] D. Schulze, Pulver und Schüttgüter, 4, Springer-Verlag, Auflage, 2019.
[90] T. Butz, Fouriertransformation für Fußgänger. 7., Aktualisierte Auflage, Vieweg+Teubner, 2011.
[91] A. Sharma, S.S. Mallick, An investigation into pressure drop through bends in pneumatic conveying systems, Part. Sci. Technol. 39 (2) (2021) 180–191.
[92] R. Pan, Improving Scale-up Procedures for the Design of Pneumatic Conveying Systems, PhD Thesis, Department of Mechanical Engineering, University of Wollongong, 1992.
[93] S.S. Mallick, Modelling of Fluidized Dense-Phase Pneumatic Conveying of Powders, PhD Thesis, Centre for bulk solids and particulate technologies – Faculty of Engineering, University of Wollongong, 2009.